ACS APPLIED MATERIALS & INTERFACES

www.acsami.org

Research Article

A Magnetosome-Based Platform for Flow Biocatalysis

Esther Mittmann, Frank Mickoleit, Denis S. Maier, Sabrina Y. Stäbler, Marius A. Klein, Christof M. Niemeyer, Kersten S. Rabe,* and Dirk Schüler*

Cite This: *ACS Appl. Mater. Interfaces* 2022, 14, 22138−22150

Read Online

ACCESS | Metrics & More | Article Recommendations | Supporting Information

ABSTRACT: Biocatalysis in flow reactor systems is of increasing importance for the transformation of the chemical industry. However, the necessary immobilization of biocatalysts remains a challenge. We here demonstrate that biogenic magnetic nanoparticles, so-called magnetosomes, represent an attractive alternative for the development of nanoscale particle formulations to enable high and stable conversion rates in biocatalytic flow processes. In addition to their intriguing material characteristics, such as high crystallinity, stable magnetic moments, and narrow particle size distribution, magnetosomes offer the unbeatable advantage over chemically synthesized nanoparticles that foreign protein "cargo" can be immobilized on the enveloping membrane via genetic engineering and thus, stably presented on the particle surface. To exploit these advantages, we develop a modular connector system in which abundant magnetosome membrane anchors are genetically fused with SpyCatcher coupling groups, allowing efficient covalent coupling with complementary SpyTag-functionalized proteins. The versatility of this approach is demonstrated by immobilizing a dimeric phenolic acid decarboxylase to SpyCatcher magnetosomes. The functionalized magnetosomes outperform similarly functionalized commercial particles by exhibiting stable substrate conversion during a 60 h period, with an average space−time yield of 49.2 mmol L^{-1} h^{-1}. Overall, our results demonstrate that SpyCatcher magnetosomes significantly expand the genetic toolbox for particle surface functionalization and increase their application potential as nano-biocatalysts.

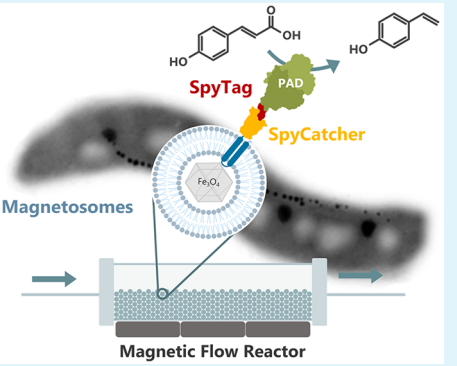

KEYWORDS: *biocatalysis, flow reactor, magnetosomes, magnetic nanoparticles, genetic engineering, bioconjugate*

INTRODUCTION

Innovative biocatalytic solutions are becoming increasingly relevant in the context of the transformation of the chemical industry.[1−5] Crucial for the application of a biocatalyst is the successful development of an overall biocatalytic process in a suitable reactor system. In this context, the principle of flow catalysis is being increasingly explored, e.g., through the use of novel reactor concepts such as biomimetic pickering emulsion reactors or self-assembling biocatalytic materials.[5−12] Specifically the use of microreactors, with dimensions ranging from microliters to milliliters, amplifies the advantages of flow systems due to the increased surface-to-volume ratio within the reactor. This allows an even better control of the reaction system and thus, higher product yields. Furthermore, microfluidics is particularly suitable for the realization of biocatalytic processes, as the frequently delicate biocatalysts are exposed to lower shear forces. In this regard, magnetic biocatalysts in a fluidized bed reactor, which are stabilized by a magnetic field, offer a straightforward approach. To enable the use of enzymes in such reactors, their immobilization is essential and can be achieved by noncovalent or covalent binding of the biocatalyst to a solid support material.[13] Using genetically encoded tags, biocatalysts can be covalently immobilized on such support materials in a predefined manner.[14−16] Thereby, the immobilization of enzymes on the surface of (nano)supports usually retains a high catalytic activity while simultaneously increasing the particle density in a reactor.[13,17−20]

An attractive alternative to the variety of commercially available nanoparticles is provided by so-called magnetosomes synthesized by magnetotactic bacteria (MTB). For instance, the alphaproteobacterium *Magnetospirillum gyphiswaldense* biomineralizes ∼40 magnetosomes per cell, consisting of a cuboctahedral core of chemically pure magnetite (Fe_3O_4) enveloped by the magnetosome membrane, a proteinaceous phospholipid bilayer.[21−23] Because of the strictly controlled biomineralization process, magnetosomes exhibit extraordinary material characteristics such as a strong magnetization, a narrow particle size distribution, and high crystallinity, to an extent that chemical synthesis can hardly achieve.[23−26] Moreover, the enveloping membrane provides sites for the covalent attachment of functional moieties.[27−29] Functionalization of the magnetosome surface can be accomplished *in vivo*

Received: February 22, 2022
Accepted: April 11, 2022
Published: May 4, 2022

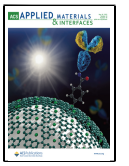

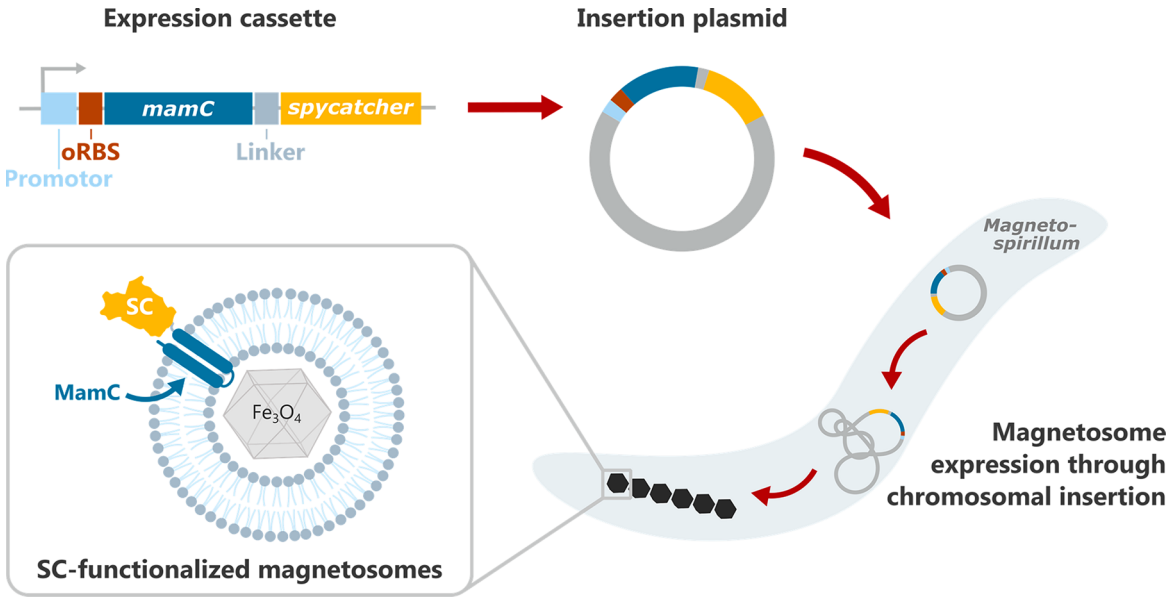

Figure 1. Biogenesis of SC-functionalized magnetosomes. Genetic organization of the expression cassette for SC display on the magnetosome surface. The *spycatcher* gene was expressed as fusion to *mamC*, with a flexible *gly-ser-thr* linker connecting both sequences. The fusion was set under the control of an optimized promoter with an optimized ribosome binding site (oRBS)[31] for constitutive high-level expression. The cassette was finally cloned into an insertion plasmid and transferred to the isogenic Δ*mamC* deletion mutant of *M. gryphiswaldense*. Stable insertion of the target sequences into the host genome by transposition enabled the production of SC-functionalized magnetosomes, which can subsequently be isolated with an intact membrane (size of particle and proteins not to scale).

by genetic engineering as well as by chemical modification of the magnetosome membrane. Although the latter is less time-consuming, such approaches lack selectivity, often require harsh reaction conditions, and are difficult to control.[30] The functionalization of the magnetosome membrane by genetic means, on the other hand, enables the specific display of functional moieties at distinct stoichiometries. Foreign "cargo" proteins are expressed as translational fusion to abundant magnetosome membrane (Mam) proteins which serve as anchor molecules. Using an optimized genetic system,[31] a variety of functionalities has been displayed on the magnetosome surface, including artificial peptides,[32−34] fluorophores,[35] or enzyme proteins,[29,36,37] demonstrating that magnetosomes have the potential to yield reusable, highly active nanobiocatalysts.

It is important to note that these functionalized particles are prearranged to specific activities and require the generation of individual genetic variants for each fusion partner. The display of versatile connectors such as nanobodies (camelid antibody fragments), biotin/streptavidin, or protein ligands could partly overcome this limitation and enabled the specific immobilization of foreign protein cargo as well as specific coupling reactions with complementary-tagged structures (such as nucleic acids) or even whole cells.[34,38−41] As such approaches are based on noncovalent interactions, they can be affected by a change in reaction conditions. Therefore, a covalent bond formation between the connector and the fusion partner would be desirable. For such approaches, the SpyTag−SpyCatcher system has recently been established.[42,43] The system consists of a 13 aa peptide tag (SpyTag, ST) and a 116 aa peptide (SpyCatcher, SC), which autocatalytically form an intermolecular isopeptide bond between an aspartate and lysine residue under a wide range of temperatures, pH values, and buffers[44] and can genetically be fused to the protein of interest. The system has been employed for a large variety of applications ranging from materials science, molecular engineering, live-cell imaging, and protein purification to synthetic biology.[7,16,45−59]

In our study, we demonstrate the installment of SC units on the surface of bacterial magnetosomes and their further functionalization with ST-modified cargo proteins. In particular, we immobilize a phenolic acid decarboxylase (PAD) as an example for a biocatalytically relevant enzyme onto the particle surface. By comparing our system with commercially available magnetic particles, also under conditions of continuous flow, we illustrate that functionalized SC-magnetosomes can serve as highly active, stable nanocatalysts for biocatalytic processes in flow reactor systems.

RESULTS AND DISCUSSION

Magnetosome Expression of SpyCatcher Connectors Generates a Flexible Adapter Scaffold. For magnetosome display of SC coupling groups, the corresponding *spycatcher* sequence from *S. pyogenes*[42,43] was optimized to the codon usage of *M. gryphiswaldense* to ensure enhanced expression and obtained in a gene-splicing reaction (Figure S1). SC moieties were expressed as translational fusion to the surface-exposed hydrophilic C-terminus of the 12.4 kDa magnetosome protein MamC, with a flexible 17 aa Gly-Ser-Thr linker connecting both sequences. MamC is tightly associated with the magnetosome membrane by its two predicted transmembrane helices[60−62] and highly abundant on magnetosome particles (80−210 copies per particle).[31,37,63] However, in magnetosome biosynthesis MamC has only a minor, nonessential function as shown by the fact that Δ*mamC* deletion cells produce wildtype (WT)-like particle numbers with only slightly reduced diameters (~95% of the WT).[64] Because of these characteristics, MamC has proven to be a suitable membrane anchor for the display of foreign proteins and peptides.[65]

https://doi.org/10.1021/acsami.2c03337
ACS Appl. Mater. Interfaces 2022, 14, 22138−22150

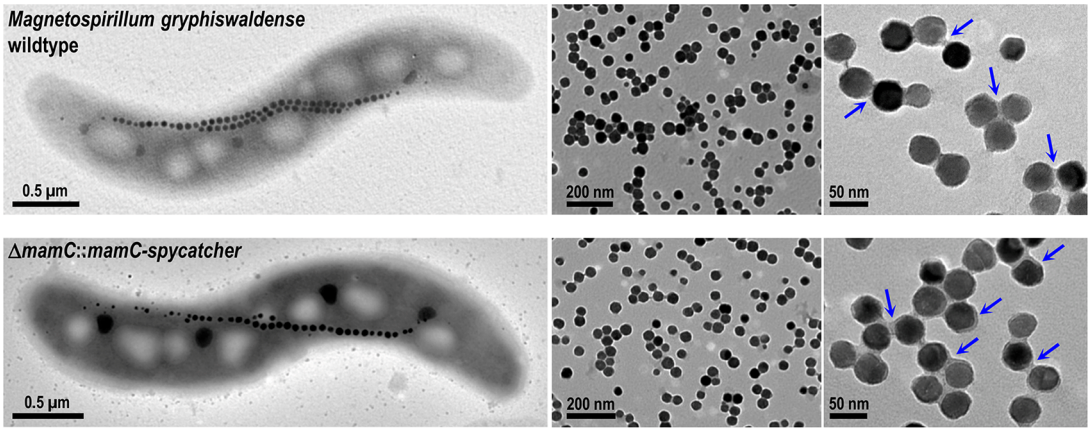

Figure 2. Transmission electron microscopy (TEM) images of a representative cell of the WT of *M. gryphiswaldense* and strain Δ*mamC*::*mamC-spycatcher*, as well as micrographs of the respective, isolated magnetosomes. The WT produced 32 ± 14 particles per cell, arranged in a chain-like manner at midcell. Suspensions of isolated particles (overall diameter 38.4 ± 6.6 nm) were free of contamination and in negatively stained preparations, an electron-light organic shell was visible (indicated by blue arrows) representing the magnetosome membrane. Genomic insertion of a *mamC-spycatcher* expression cassette into the Δ*mamC* deletion mutant fully complemented the WT phenotype. The resulting strain Δ*mamC*::*mamC-spycatcher* biomineralized 32 ± 10 magnetosomes per cell with an overall diameter of 41.6 ± 7.3 nm. As in the WT, isolated particles were enveloped by an organic shell of ∼5 nm on average in thickness.

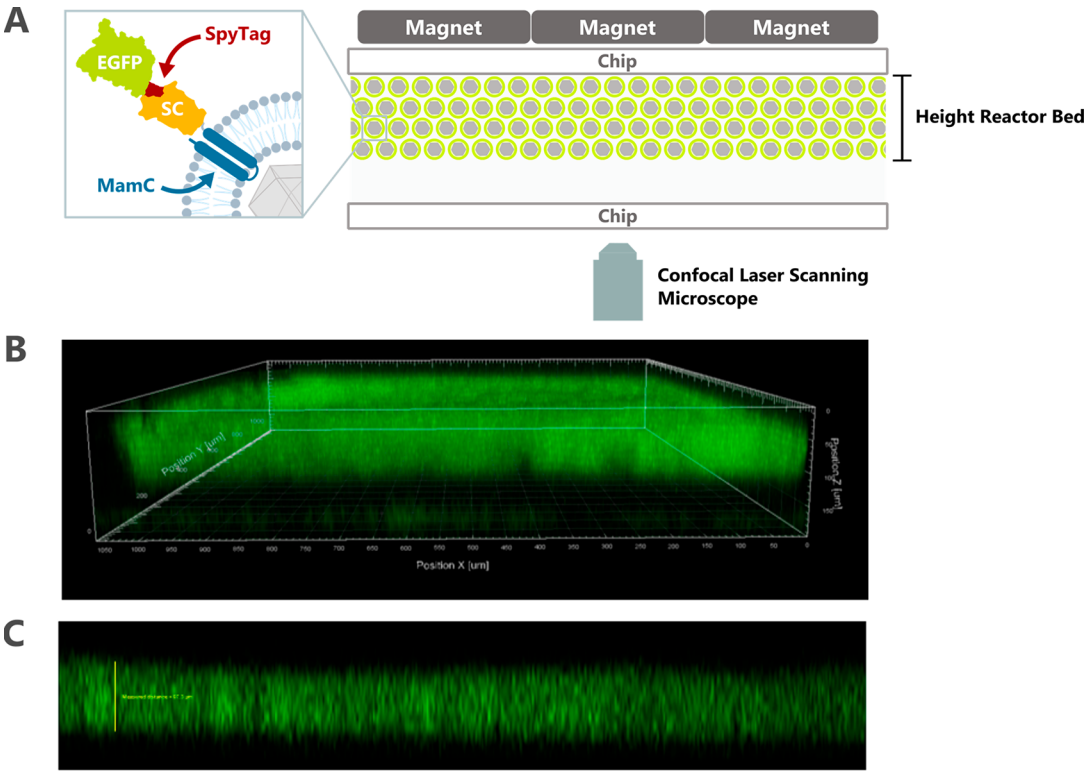

Figure 3. (A) For fluorescence microscopic analysis the SC-magnetosomes were functionalized with ST-modified EGFP[16] and loaded into a Topas chip with straight channels. The channel was closed and the chip was mounted on a chip holder with integrated Nd magnets. Note that due to the hardware configuration, the magnets of the chip holder are at the top of the channel. After placement of the setup in a fluorescence microscope (LSM 880 with Airyscan, Zeiss) the EGFP fluorescence was analyzed. (B) A *z*-stack of the channel segment allows a 3D-view of the channel. (C) The layer thickness of the magnetosomes in the channel was determined by measuring the fluorescence in the *z*-view of the image.

The MamC−SpyCatcher fusion protein was expressed under control of the strong constitutive magnetosomal $P_{mamDC45}$ promoter with an optimized ribosome binding site (oRBS),[31] as illustrated in Figure 1. The isogenic Δ*mamC* mutant strain of *M. gryphiswaldense* was chosen as recipient for the gene fusion, resulting in strain Δ*mamC*::*mamC-spycatcher*.

Magnetosome biosynthesis and cell morphology was not affected by *spycatcher* expression, and strain Δ*mamC*::*mamC-spycatcher* biomineralized 32 ± 10 particles per cell arranged in a chain-like manner at midcell (Figure 2). For isolated SC-displaying magnetosomes (termed SC-magnetosomes) an overall average diameter of 41.6 ± 7.3 nm was measured from TEM micrographs, with an electron-light, organic shell of ∼5 nm representing the magnetosome membrane surrounding the magnetite cores.

https://doi.org/10.1021/acsami.2c03337
ACS Appl. Mater. Interfaces 2022, 14, 22138−22150

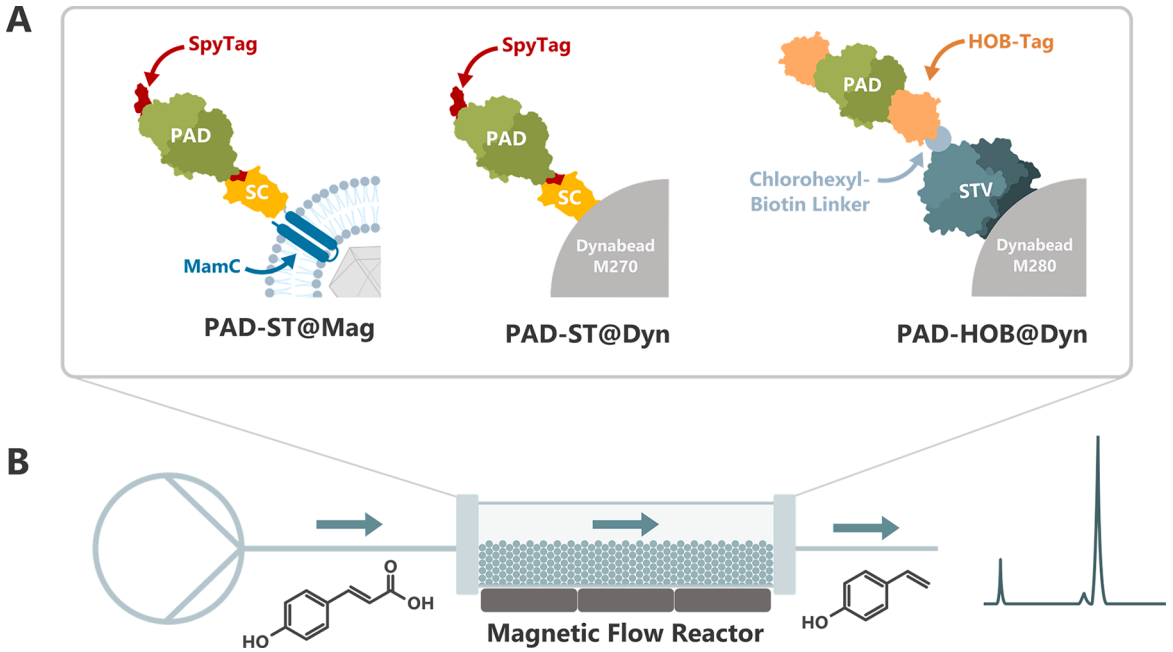

Figure 4. (A) SC-functionalized magnetosomes can be used as immobilizable nano-biocatalysts by coupling ST-equipped monomers of the dimeric phenolic acid decarboxylase (PAD-ST) onto the SC-magnetosome surface (PAD-ST@Mag). This approach was compared with the immobilization of the PAD on SC-modified, commercially available Dynabeads M270 Epoxy (PAD-ST@Dyn) and PAD-HOB fusion protein immobilized via a chlorohexyl−biotin linker on commercially available streptavidin-coated Dynabeads STV M280 (PAD-HOB@Dyn) for the conversion of *p*-coumaric acid to *p*-hydroxystyrene in a magnetic microreactor in flow (B).

The presence of MamC−SpyCatcher in the isolated magnetosome fraction was confirmed by denaturing PAGE and Western blotting, followed by immunochemical detection employing IgG antibodies specific for MamC (Figure S2). For WT particles or SC-magnetosomes, the expected protein bands were detected, with electrophoretic mobilities corresponding to molecular masses of ∼13 and ∼30 kDa, respectively (calculated masses: 12.4 kDa for MamC and 26.2 kDa for MamC−SpyCatcher).

The functionality, i.e., the capability to bind complementary ST-equipped proteins, as well as the amount of SC molecules displayed on the particle surface was investigated by incubating SC-magnetosomes with different amounts of recombinantly produced EGFP-ST. Both fluorescence microscopy analysis and Western blotting (Figure S3) indicated saturation of the SC adapter scaffold at ∼60 μg of EGFP-ST per mg of iron. Taking into account the molecular mass of the EGFP-ST fusion (31.4 kDa) and the mass of a single magnetosome particle, an average copy number of ∼170 EGFP-ST moieties can be calculated to be present on each SC-magnetosome (for details on the calculation see the supplementary discussion to Figure S3). This value is in accordance with previous reports, in which the average copy number of MamC, and consequently the number of functional moieties on the magnetosome surface, was estimated to be within the range from 80 to 210 molecules.[31,37,63] Our observations therefore clearly show the successful immobilization of functional EGFP-ST (as a foreign cargo protein) on the surface of SC-magnetosomes and complete saturation of the SC-magnetosome adapter scaffold with all MamC−SpyCatcher fusions being covalently linked to EGFP-ST.

The isolated SC-magnetosomes provide a versatile carrier material for the selective immobilization of functional cargo. To gain a better understanding of magnetosome behavior in a magnetic bioreactor, EGFP@Mag (i.e., SC-magnetosomes displaying ST-modified EGFP) were loaded into a linear reactor channel. The thickness of the layer in the channel was analyzed by using a *z*-stack of EGFP fluorescence in a fluorescence microscope (Figure 3).

Representative measurements of the magnetosomes in the channel showed a layer thickness of ∼97 μm, which is in the same range as the previously reported layer thickness of biotin-Atto647-functionalized STV Dynabeads with ∼86 μm.[66] This result suggests that a similar amount of carrier material can be loaded into the reactor channel. However, the size of the carrier material has to be considered, as the use of smaller particles leads to an increase in the effective reactor surface area and, thus, a higher number of functional units in an equal reactor volume, potentially leading to a significant enhancement in reactor efficiency. After removal of the underlying Nd magnets, the EGFP-ST@Mag were readily flushed out without visible aggregation.

Comparison of PAD-ST Immobilized on SC-Magnetosomes with PAD Immobilized on Dynabead Architectures. To benchmark the use of magnetosomes as immobilization matrix for flow biocatalysis, we chose the previously described dimeric phenolic acid decarboxylase (PAD) from *Enterbacter sp.* as a well-established biocatalyst, which offers a sustainable route to styrene derivatives from biologically derived phenolic acids.[46,67,68]

Three different particle systems were compared for the immobilization of the PAD in this study (Figure 4A), and their performance in flow microreactors stabilized by a magnetic field was investigated (Figure 4B). For this purpose soluble, heterologously expressed ST-equipped PAD (PAD-ST)[46] was coupled onto the surface of SC-magnetosomes to yield PAD-ST@Mag. This approach was compared with the immobilization of the enzyme on modified, superparamagnetic Dynabeads

https://doi.org/10.1021/acsami.2c03337
ACS Appl. Mater. Interfaces 2022, 14, 22138−22150

with a size of 2.8 μm (Figure 4A). Dynabeads are commercially available, composite magnetic support materials with various surface chemical modifications and coatings. They have been shown to provide high mechanical stability and low porosity as well as excellent biocompatible properties.[14,69−71] Dynabeads M-270 Epoxy beads were covalently functionalized with heterologous expressed and purified SC protein as previously reported.[14] Subsequently, incubation with PAD-ST led to capture of the enzyme and yielded the immobilized biocatalyst PAD-ST@Dyn. As an alternative example for a self-immobilizing PAD fusion enzyme, the HOB-tag was investigated for its suitability to immobilize the PAD, resulting in PAD-HOB@Dyn. The HOB-tag, a variant of the HaloTag, is a self-ligating fusion tag that binds covalently to chlorohexyl (CH) suicide ligands[72,73] and was genetically attached to the PAD at its C-terminus. To employ this fusion enzyme, we used Dynabeads M-280 streptavidin, which were further modified with a biotin−PEG−chlorohexyl linker as previously reported.[14,66] A detailed scheme of the synthesis routes for each catalyst can be found in Figure S4.

There are several relevant considerations for a valid assessment of the efficiency of immobilized biocatalysts in a flow reactor. A potentially detrimental influence of the binding tags on the biocatalyst's activity has to be investigated. However, we found that the fusion of PAD with the tags used in this work could be heterologously expressed in high purity (Figure 5A) with no significant differences in the substrate conversion rate (Figure 5B). Furthermore, maximizing the volumetric activity of flow reactors is a crucial parameter for their efficiency and strongly depends on the effective surface area and binding capacity of the support matrix used. Prior to application in a flow process, the PAD activity per milligram of carrier material was analyzed via the conversion of *p*-coumaric acid (*p*CA) to *p*-hydroxystyrene (*p*HS) in a batch assay. PAD-ST@Mag showed a superior activity per milligram of carrier material in comparison to PAD-ST@Dyn and PAD-HOB@Dyn (Figure 5C), which might be due to the higher surface area of the magnetosome nano-biocatalyst in comparison to the Dynabeads.

Application of PAD-ST@Mag in a Miniaturized Continuous Flow Biocatalysis. We next investigated the operational stability of the three immobilized PAD biocatalysts in a flow process. For practical processes it is important that the immobilized enzyme preserves high catalytic activity over a prolonged time. To this end, the different magnetic biocatalysts were loaded into a microreactor and fixed via Nd magnets incorporated in the reactor holder in a continuous reaction format with automated sampling (Figure 6A,B). We chose a flow rate of 1 μL min^{-1}, leading to a typical residence time of 3.5 min. Similar to the experiments performed in batch mode, the immobilized decarboxylase biocatalysts exhibited excellent activity (Figure 6C). Employing 2 mg of PAD-ST@Mag, near-quantitative conversion to *p*HS was achieved during the first 24 h. PAD-ST@Mag proved to be more durable than the PAD immobilized on Dynabeads, leading to an average space−time yield (STY) of 49.2 mmol L^{-1} h^{-1} during a run time of 60 h. The use of 2 mg of PAD-ST@Dyn led to a satisfactory average STY of 44.7 mmol L^{-1} h^{-1}. In contrast, no full conversion could be obtained when employing 2 mg of PAD-HOB@Dyn. The activity significantly declined after 14 h, leading to an average STY of only 30.1 mmol L^{-1} h^{-1} in the course of 60 h. The decrease in activity in the case of the PAD-HOB@Dyn was expected, since the PAD-HOB is covalently

Table 1. Architectures of Magnetic Decarboxylase Biocatalysts Used in This Study

biocatalyst	PAD-ST@Mag	PAD-ST@Dyn	PAD-HOB@Dyn
PAD variant	PAD-ST	PAD-ST	PAD-HOB
carrier material	SC-magnetosomes	SC-modified Dynabeads M-270 Epoxy	CH-modified Dynabeads M-280 STV
particle size	41.6 ± 7.3 nm	2.8 μm	2.8 μm
surface properties	biogenic, membrane-enveloped magnetite nanoparticles with surface-exposed SC, genetically incorporated and immobilized as translational fusion with the magnetosome membrane anchor MamC	nonporous, pH neutral, hydrophilic, epoxy-activated magnetic particles[74] with immobilized SC-protein	nonporous, hydrophobic, tosyl-activated magnetic particles with immobilized BSA and STV,[75] further functionalized with a biotin−chlorohexyl linker

https://doi.org/10.1021/acsami.2c03337
ACS Appl. Mater. Interfaces 2022, 14, 22138−22150

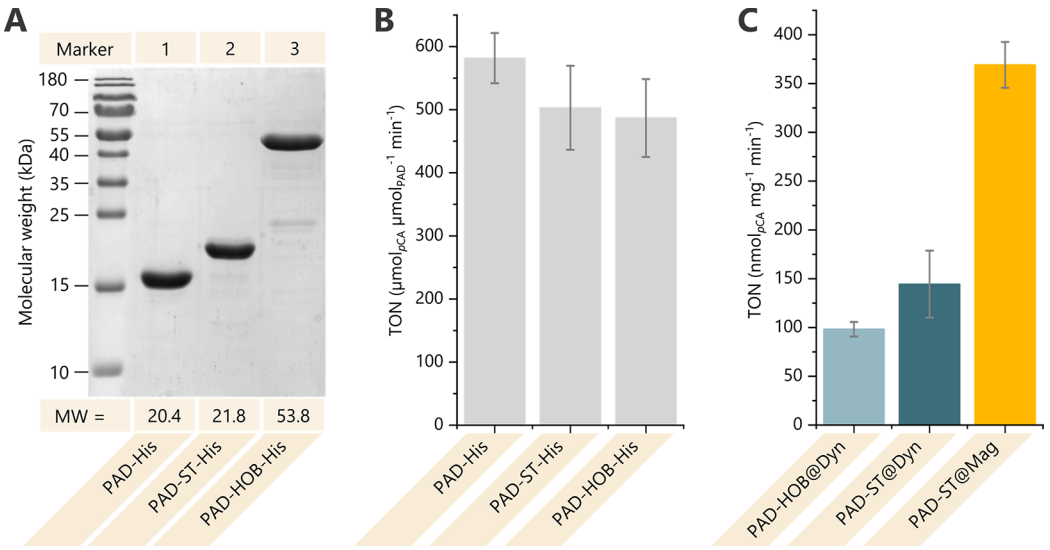

Figure 5. Characterization of PAD-fusion proteins and immobilized PAD on different carrier materials. (A) Denaturing 16% SDS-PAGE analysis of 4 μg of each PAD fusion protein after heterologous expression in *E. coli* and purification via a C-terminal 6×His-tag. The proteins were obtained in purities >95% according to grayscale analysis. Lane 1: PAD (20.4 kDa); Lane 2: PAD-ST (21.8 kDa); Lane 3: PAD-HOB (53.8 kDa); Marker: PageRuler prestained protein ladder (Thermo Scientific). Molecular weight of to the monomer is given. (B) Enzymatic activity in (μmol$_{pCA}$ μmol$_{PAD}^{-1}$ min^{-1}) of the PAD variants by using 0.1 mM *p*-coumaric acid (*p*CA) as substrate, determined by an absorbance-based assay in PAD Buffer (25 mM potassium phosphate buffer, pH 6) at 30 °C. (C) Specific activities per milligram of carrier material of PAD-functionalized SC-magnetosomes (PAD-ST@Mag; yellow) in a batch reaction in comparison to the alternative magnetically immobilizable biocatalyst systems. The conversion of *p*CA to *p*HS through PAD-ST@Mag, PAD-ST immobilized on SC-Dynabeads (PAD-ST@Dyn; dark blue), or PAD-HOB immobilized on CH-Dynabeads (PAD-HOB@Dyn; light blue) was monitored at different points in time by using HPLC analysis. All experiments were performed in PAD-Buffer at 30 °C and 600 rpm at least in duplicates by using different batches of magnetosomes or particles.

coupled to the chlorohexyl−biotin, but its binding to the streptavidin is noncovalent, leading to a constant removal of PAD from the reactor bed.

The slow decline in reactivity of the PAD-ST@Mag could potentially be due to disintegration of the magnetosomes. However, we could not detect obvious changes in magnetosome morphology when comparing particles before and after application in the flow reactor (Figure S5). On the contrary, the stability of the PAD appears to be improved by immobilization. While a flow reactor loaded with only 50 μg of PAD-ST@Mag still showed more than 65% of its initial activity after 96 h, the free PAD-ST in the working stock concentration for the batch assays under comparable conditions (30 °C, PAD reaction buffer) lost most of its activity after 96 h with only 7% of its initial activity remaining (Figure S6). Therefore, the loss in activity over time might indicate a loss of particles. These could, however, be recovered and recirculated into the reactor. In comparison with the available commercial particle systems, the magnetosome-based system developed here provides high space−time yields in flow biocatalytic applications, while offering a platform for the modular decoration of magnetic nanoparticles requiring no chemical functionalization reactions.

CONCLUSION

Magnetosomes are a biologically produced alternative to existing commercial, magnetic beads for the immobilization of target proteins, such as biocatalysts. Genetic engineering provides a highly selective and reliable tool for the (multi)-functionalization of the magnetosome surface;[29,31,65] however, its time-demanding nature (i.e., the generation of strains producing functionalized magnetosomes) lowers the throughput, and generated particles are predetermined to distinct functionalities. Widely used *in vitro* approaches such as cross-linking reactions allow for a much more rapid functionalization of the particle surface but lack specificity and controllability.[30] In our study, we combined the advantages of both *in vivo* and *in vitro* functionalization by magnetosome expression of a covalent MamC−SpyCatcher bioconjugate and subsequent coupling of SpyTagged protein cargo. While there are many synthetic strategies available for interconnecting two protein compounds, including split inteins,[76] coiled coils,[77] and split proteins,[78] the ST−SC system provides a strong and irreversible interaction by spontaneous reconstitution of an intramolecular isopeptide bond.[43]

Immobilization of ST-equipped PAD monomers on the SC-magnetosome surface resulted in catalytically highly active nanoparticles that could be applied as nano-biocatalyst in a flow reactor system. Compared to likewise functionalized commercial Dynabeads, magnetosomes exhibited more stable conversion rates and an overall increased activity, which might be explained by the smaller magnetosome diameter. Thus, a significantly higher number of functional moieties can be immobilized on the same amount of carrier material, making magnetosomes well-suited for flow catalysis. The simultaneous fusion of the SC bioconjugate to several different magnetosome proteins could further enhance the SC protein density on the particle surface. In addition, the simultaneous fusion of SC moieties to the N- and C-termini of the respective membrane anchors, or even as arrays,[37] might drastically increase the binding capacity of the particles, thereby turning the magnetosome membrane into a more flexible multimodal binding platform for functional moieties. The catalytic activity of the functionalized magnetosomes furthermore suggests the correct dimerization of the PAD monomers as it has been observed for genetically engineered, enzyme displaying

https://doi.org/10.1021/acsami.2c03337
ACS Appl. Mater. Interfaces 2022, 14, 22138−22150

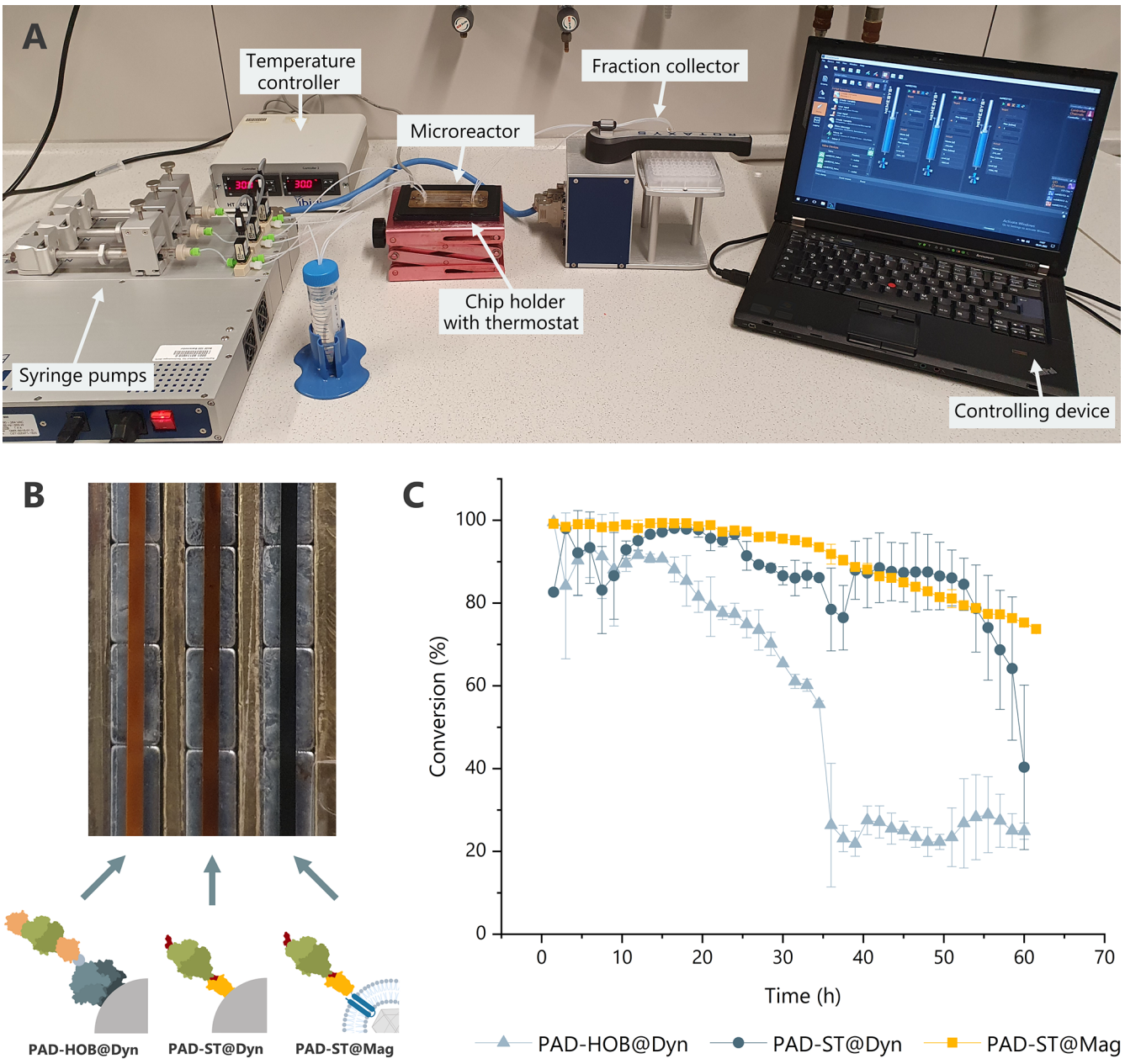

Figure 6. Application of the PAD-functionalized SC-magnetosomes in continuous flow reactors in comparison with the alternative magnetically immobilizable biocatalyst systems (Dynabeads). (A) Fluidics setup used in this study. Glass syringes containing the substrate solutions were installed in Cetoni Nemesys syringe pumps and connected to a Topas chip with four straight channels via PTFE tubing. The chip was mounted on a brass chip holder with integrated Nd magnets to retain the magnetic catalyst, and the chip holder was connected to a thermostat for temperature control. The reactor outflow was automatically fractionated into a 96-well plate by using a Cetoni rotAXYS positioning system, modified for parallel sampling of up to three samples. (B) Magnetic microfluidic packed-bed reactor loaded with PAD-functionalized magnetic particles. The picture shows three channel compartments. The brass chip holder is connected to a thermostat to control the temperature and contains integrated rectangular Nd magnets that retain the PAD-functionalized magnetic carriers. The first channel on the left contains the light brown PAD-HOB@Dyn, while the dark brown PAD-ST@Dyn is applied in the center. The right channel contains the black PAD-ST@Mag. (C) Conversion of *p*CA to *p*HS over 60 h in flow microreactors using PAD-ST@Mag (yellow), PAD-HOB@Dyn (light blue), and PAD-ST@Dyn (dark blue). All experiments were performed at least in duplicates by using different batches of magnetosomes and particles. The reactors were perfused with 1 μL min^{-1} of a 5 mM *p*CA substrate solution in PAD buffer at 30 °C. Fractions were automatically collected every 90 min, and the substrate conversion was determined via HPLC analysis of the reactor outflow.

magnetosomes.[29,37] Moreover, an increased enzymatic stability of PAD-ST was observed (compared to the soluble enzyme), suggesting that the immobilization on the magnetic carrier facilitates and stabilizes folding and dimerization of the enzyme. Because of the flexibility of the ST−SC system, the study performed here opens the door to applications employing many other biocatalytically relevant enzymes. Thereby, the magnetosome system might be especially useful for enzymes, which prefer the presence of membranes for their immobilization.

In summary, the display of SC connectors greatly enhances the flexibility to functionalize the magnetosome surface with

https://doi.org/10.1021/acsami.2c03337
ACS Appl. Mater. Interfaces 2022, 14, 22138−22150

foreign protein cargo and extends the existing toolkit of magnetosome-adapted coupling groups (such as nanobodies or streptavidin[38,39,79]). Because the complementary ST-peptide tag can be easily fused with the desired protein function, the ST−SC system could enable the functionalization of the magnetosome surface with any foreign proteins, thereby greatly facilitating the fabrication of multifunctional magnetic nanoparticles with tailored properties.

EXPERIMENTAL SECTION

Bacterial Strains and Cultivation Conditions. Bacterial strains that were used in this study are listed in Table S1. *M. gryphiswaldense* strains were cultivated microaerobically (to induce magnetite biomineralization) in modified flask standard medium (FSM) under moderate shaking (120 rpm) at 28 °C as described previously.[80,81] *Escherichia coli* strains were grown as described previously.[31,37,68] For cultivating *E. coli* WM3064 [Metcalf, W., unpublished] DL-α,ε-diaminopimelic acid (DAP) was added to lysogeny broth (LB) medium at a final concentration of 1 mM. Solid media were prepared by adding 1.5% (w/v) agar; for strains carrying recombinant plasmids, media were supplemented with 20 μg mL^{-1} chloramphenicol (Cm) and/or 25 μg mL^{-1} kanamycin (Km) or 100 μg mL^{-1} ampicillin (Amp) for *E. coli*, or 5 μg mL^{-1} for *M. gryphiswaldense* strains.

Molecular and Genetic Techniques. Oligonucleotides (Table S2) were purchased from Sigma-Aldrich (Steinheim, Germany). Plasmids used in this study are listed in Table S3. Plasmids were constructed by standard recombinant techniques as described in detail below.

Construction of pET22-EsPAD-HOB-His. The genetic construction was performed by using the *in vitro* recombination method described by Gibson et al.[82] utilizing PCR products and synthetic DNA fragments with 30 bp homologous overlaps. For the generation of PAD-HOB-His, the backbone encoding for a N-terminal PAD and C-terminal 6×His-Tag separated by a glycine spacer was amplified and linearized by using primers EM01 and EM02 with pET22-EsPAD-SC-His[46] as template. This backbone was then recombined with a HOB encoding insert, which had been generated by polymerase chain reaction (PCR) by using the primers EM09 and EM10 with pET22-Gre2-HaloStar-His[14] as template. After assembly, DpnI digests were performed, and the reaction mixtures were transformed into chemically competent *E. coli* NEB5-alpha cells (New England Biolabs). Plasmid DNA was isolated by using the ZR Plasmid Miniprep - Classic Kit from Zymoclean according to the manufacturer's instructions. The correct assembly and sequence of the resulting plasmids were verified by commercial sequencing (LGC Genomics, Germany).

Construction of pET28A-His-EGFP-ST. The pET28a-His-EGFP-ST expression vector was constructed by fusing the *spytag* sequence to the sequence of the EGFP reporter protein, prior to cloning the fusion into the multiple cloning site of pET28a (Novagen, Darmstadt, Germany). *egfp* was amplified from pJH2 by using primers GFP-NdeI-fwd and GFP-Linker-SpyTag-rev, thereby generating a NdeI restriction site upstream of *egfp* and fusing a sequence consisting of a 17 amino acid *gly-ser-thr* linker and the *spytag* to the *egfp* gene. The resulting fragment was subsequently amplified by using primers GFP-NdeI-fwd and SpyTag-rev to generate a *Bam*HI restriction site downstream of the *spytag* sequence. Afterward, the *egfp-spytag* fusion was inserted into NdeI and *Bam*HI restriction sites of pET28a.

Construction of *M. gryphiswaldense* Strain Δ*mamC*::*mamC-spycatcher*. The sequence of CnaB2 was taken from the UniProt database (www.uniprot.org; UniProtKB - Q6A1F3) and modified/optimized as described by Zakeri et al.,[43] thereby changing amino acids I34 and M69. The ST and SC sequences were obtained by dissection of CnaB2 into a 13 aa peptide representing the C-terminal β-strand and a 138 aa protein as reaction partner.[42,43] Because of a divergent %GC content (*M. gryphiswaldense*, 62%;[31] *S. pyogenes*, 38.5%[83]), which was expected to compromise expression in *M. gryphiswaldense*, the *spytag* and *spycatcher* genes were optimized to the codon usage of *M. gryphiswaldense*. For reverse translation and codon optimization, the SMS (Sequence Manipulation Suite, www.bioinformatics.org) was used. SC moieties were expressed as translational fusion to MamC, which served as membrane anchor. For that purpose, the *spycatcher* sequence was fused to *mamC* with a 17 amino acid *gly-ser-thr* linker (TSGGSGGTGGSGGTGGS)[40,84] connecting both sequences. The *spycatcher* gene was obtained by overlap PCR[85] by using the fragments SpyCatcher-1 to SpyCatcher-4 (Figure S1A). The resulting fragment was subsequently amplified by PCR by using primers Linker-SpyCatcher-fwd and SpyCatcher-rev, thereby fusing the 17 amino acid linker to the *spycatcher* sequence and generating NcoI and *Bam*HI restrictions sites up- and downstream of the construct (Figure S1B). The latter was subsequently inserted into the NcoI and *Bam*HI restriction sites of pSB9 (downstream of *mamC*), resulting in pFMDM1. The isogenic Δ*mamC* strain of *M. gryphiswaldense* was conjugated with pFMDM1, and the *mamC-spycatcher* expression cassette ($P_{mamDC45}$_*mamC-spycatcher*, Figure S1C) was inserted into the chromosome at random position by Tn5 transposition.

Magnetosome Isolation. Magnetosomes were isolated from microaerobically grown *M. gryphiswaldense* cultures as described previously.[63,86] Briefly, the cells were harvested by low-spin centrifugation, resuspended in 50 mM HEPES/NaOH + 1 mM EDTA, pH 7.2, and disrupted by using a microfluidizer system. Particle isolation and purification were achieved by subjecting the obtained crude extract to MACS magnetic separation columns (5 mL; Miltenyi, Bergisch Gladbach, Germany) placed between two neodymium−iron−boron magnets. After several washing steps, the magnetic field was removed, and the magnetosomes were eluted from the column. As an additional purification step, the magnetosome suspension was afterward centrifuged through a 60% (w/v) sucrose cushion at 200000*g* for 2 h at 4 °C. Finally, after resuspending the magnetosome pellet, the suspension was stored in Hungate tubes at 4 °C under a nitrogen atmosphere.

Heterologous Expression in *E. coli* and Purification of the Proteins PAD, PAD-ST, PAD-HOB, and SC. *E. coli* BL21(DE3) cells were transformed with the plasmid pET22-EsPAD-His,[68] pET22-EsPAD-ST-His,[46] pET22-EsPAD-HOB-His, pExp1-His-SC or ST-EGFP-His[16] using heat shock. The cells were selected overnight on LB/agar plates containing 100 μg mL^{-1} ampicillin at 37 °C. Individual clones were used to inoculate liquid cultures of 100 mL of LB medium supplemented with 100 μg mL^{-1} ampicillin (LB+Amp) and cultured overnight at 37 °C and 180 rpm. Erlenmeyer flasks with LB+Amp were inoculated 1:40 with the respective overnight culture. The cultures were incubated at 37 °C and 180 rpm until an OD_{600} of 0.6 was reached. Subsequently, the culture was cooled to 25 °C for at least 15 min, and protein expression was induced with 0.5 mM isopropyl-β-D-thiogalactopyranoside (IPTG). For PAD-HOB an alternative protocol was used: Here, protein expression was induced with 0.1 mM IPTG at an OD_{600} of 1.0. After incubation at 25 °C overnight the cells were harvested by centrifugation (10000*g*, 10 min, 4 °C), resuspended in NPI10 buffer (50 mM NaH_2PO_4, 500 mM NaCl, 10 mM imidazole, pH 8) and frozen at −80 °C until further processing. The proteins were purified via NTA chromatography using His60 Ni Superflow Cartridges (Clontech) mounted on an Äkta Pure liquid chromatography system (GE Healthcare, Germany) as previously described.[46] Subsequently, the buffer was exchanged to PBS buffer (11.5 mM sodium phosphate, 500 mM NaCl, pH 7.5) by using Vivaspin Turbo 15, 10000 MWCO or 5000 MWCO (Sartorius), depending on the size of the protein.

Heterologous Expression in *E. coli* and Purification of Recombinant EGFP-ST Protein. For high-level production of recombinant EGFP-ST, the respective pET28a expression vector (Table S3) was transformed into competent *E. coli* Rosetta (DE3). A positive clone carrying the construct was cultivated aerobically at 37 °C in 1.0 L of LB medium supplemented with Cm/Km. Expression of the ST fusion protein was induced at an optical density OD_{600} of ∼0.6 with 1.0 mM IPTG. Crude extracts were ultracentrifuged (2.5 h at 100000*g*, 4 °C; Thermo Scientific Sorvall WX Ultra 80 with rotor 45 Ti (Waltham, MA)) to remove cellular debris and membranes. The resulting cytoplasmic fractions contained high amounts of EGFP-ST

https://doi.org/10.1021/acsami.2c03337
ACS Appl. Mater. Interfaces 2022, 14, 22138−22150

and were stored at 4 °C until further use. The pET28a expression vector enabled the high-yield production of recombinant EGFP-ST, equipped with an N-terminal 6×His-Tag. The latter allowed efficient purification by Ni-NTA chromatography using 1 mL fast-flow nickel columns (GE Healthcare, Chalfont St. Giles, UK) and applying a bind−wash−elute procedure.[87,88] A constant flow rate of 1 mL min^{-1} was ensured by employing a Pharmacia LKB P-1 peristaltic pump (Uppsala, Sweden). Prior to loading the cytoplasmic fraction (which contained the soluble, His-tagged EGFP-ST protein) onto the column, the latter was washed with 10 column volumes of ddH_2O and 5 column volumes equilibration buffer (50 mM NaH_2PO_4 + 0.5 M NaCl, pH 7.4). After subjecting the cytoplasm to the column, a stepwise imidazole gradient (1, 2.5, 5, 10, 50, 100, and 500 mM imidazole in equilibration buffer) was used to elute and fractionate the proteins bound to the column.

Preparation of PAD-Functionalized SC-Magnetosomes (PAD-ST@Mag). Magnetosomes were stored in ddH_2O at 4 °C prior to use. Prior to enzyme immobilization, the particles were washed three times with PAD buffer (25 mM potassium phosphate, pH 6). For enzyme immobilization, 2 nmol of ST-labeled protein was mixed in 1.8 mL of PAD buffer per mg of magnetosomes for 60 min at 30 °C in a rotator. The magnetosomes were magnetically retained and washed three times with PAD buffer. The beads were immediately used.

Preparation of SpyCatcher-Modified Dynabeads Functionalized with PAD-ST (PAD-ST@Dyn). Magnetic beads displaying the SC on the surface (SC-Dyn) were generated as previously described[14] following the manufacturer's instructions. For enzyme immobilization, 1 nmol of purified ST-labeled protein was mixed in 1.8 mL of PAD buffer per mg of SC-Dyn at 30 °C for 60 min in a rotator. The Dynabeads were washed three times with PAD-T-buffer (PAD buffer supplemented with 0.01% Tween-20). The beads were used immediately.

Preparation of Chlorohexyl-Modified Dynabeads Functionalized with PAD-HOB (PAD-HOB@Dyn). For the immobilization of HOB-tagged EsPAD, chlorohexyl-modified magnetic particles were prepared as previously described.[14] In brief, Dynabeads M-280 streptavidin beads were incubated with the biotin−PEG−chlorohexyl conjugate (HaloTag PEG-Biotin Ligand, Promega) dissolved in 100 mM potassium phosphate buffer pH 7.5 to a final concentration of 2 nmol of biotin−PEG−chlorohexyl conjugate per mg of bead and mL of buffer. The suspension was incubated for at least 60 min at 30 °C in a tube rotator, and the beads were magnetically retained and washed with PAD-T-Buffer. For enzyme immobilization, 1 nmol of purified PAD-HOB was mixed in 1.8 mL of enzyme buffer per mg of CH-Dyn for 60 min at 30 °C in a rotator. The Dynabeads were washed three times with PAD-T-Buffer and used immediately.

Flow Biocatalytic Experiments. The PAD-functionalized magnetic particles were loaded into the individual compartments of a four straight channel Topas chip (microfluidic ChipShop, Jena, Germany) through a homemade pipet adapter and a correspondingly loaded pipet tip by using a negative flow rate of −20 μL min^{-1}. The dimensions of each channel are 58.5 × 1.0 × 0.2 mm^3, which corresponds to a total reactor volume of 11.7 μL and ∼10 μL of area with underlying Nd permanent magnets. Successful loading of the reactor was monitored by visual inspection. Filled channels were connected with a short PTFE tubing (internal diameter 0.5 mm) to connect the chip inlet with a CETONI neMESYS syringe pump containing the substrate solution and the chip outlet with the CETONI Compact Positioning System rotAXYS. The reactor temperature was maintained at 30 °C via a HT200 temperature-controlled chip holder (ibidi GmbH, Germany), in which a brass chip holder modified with Nd permanent magnets for retention of the catalyst was mounted. The syringe pump was filled with 5 mL of substrate solution containing 5 mM *p*CA supplemented with 0.01% sodium azide in PAD buffer. A flow rate of 1 μL min^{-1} was used. The chip effluent was automatically fractionated by the rotAXYS system in a 96-well plate containing 60 μL of acetonitrile, supplemented with aqueous HCl and cinnamic acid as internal standard to stop all enzymatic reactions. The samples were then analyzed by HPLC as described in the following sections.

Analytical Methods. Cellular growth of *M. gryphiswaldense* strains was monitored photometrically by measuring the optical density at 565 nm (OD_{565}). Magnetosome production was estimated by determining the magnetic response (C_{mag}) of the cultures when subjected to different magnetic field orientations (tilted by 90°). The ratio of the scattering intensities relative to the light beam correlates with the average particle numbers, allowing semiquantitative estimations of the magnetosome contents.[89]

Transmission electron microscopy (TEM) of whole cells or isolated magnetosomes was performed on a CEM 902A (Zeiss, Oberkochen, Germany) with an acceleration voltage of 80 kV. Images were taken with a Gatan Erlangshen ES500W CCD camera. Samples were prepared as previously described.[86] Crystal sizes were measured with ImageJ software.[90] TEM analyses for investigations regarding the morphology of PAD-ST@Mag before and after flow reaction were performed on an EM910 transmission electron microscope (Zeiss, Oberkochen, Germany) with an acceleration voltage of 80 kV.

Iron contents of suspensions of isolated magnetosomes were determined by flame atomic absorption spectroscopy (AAS). 50−100 μL of the corresponding suspensions was mixed with 69% nitric acid to a final volume of 1 mL and digested at 98 °C for 3 h. Afterwards, the samples were filled up with ddH_2O to a volume of 3 mL and analyzed by using an Analytik Jena contrAA300 high-resolution atomic absorption spectrometer (Analytik Jena, Jena, Germany) as described previously.[86] Iron contents are given as mean values and represent the averaged values of three experiments measured in quintuplicates.

Protein concentrations were determined via UV−vis spectroscopy using the theoretical molar extinction coefficients at 280 nm, as calculated by the Geneious ver. 8.1.9 software.

For fluorescence microscopy, an LSM 880 with Airyscan (Zeiss, Oberkochem, Germany) was used.

Coupling of recombinantly expressed, soluble EGFP-ST to isolated SC-magnetosomes was assessed by measuring the fluorescence intensity by using excitation/emission wavelengths of 485/535 nm, respectively, in an Infinite M200pro plate reader (Tecan, Crailsheim, Germany). To allow comparison between different samples, fluorescence intensities were normalized to their respective iron concentrations.

Denaturing Polyacrylamide Gel Electrophoresis (PAGE) and Western Blotting. For analyzing the protein purifications, the respective samples were incubated with loading buffer containing 100 mM β-mercaptoethanol for 10 min at 95 °C ("harsh" denaturing conditions), separated by electrophoresis according to the method described by Laemmli[91] and stained with Coomassie Brilliant Blue G-250. PageRuler Prestained Protein Ladder (Thermo Fisher Scientific) served as reference marker. Samples of isolated magnetosome suspensions were mixed with loading buffer containing 100 mM DTT and incubated at room temperature for 10 min ("mild" denaturing conditions). The solubilized magnetosome membrane protein fractions were separated by electrophoresis according to Fling and Gregerson[92] and subsequently transferred onto polyvinylidene difluoride (PVDF) membranes (Roth, Germany). Immunochemical detection was performed as previously described[37,40] by using a primary rabbit IgG antibody specific for MamC at a ratio of 1:1000 and secondary goat anti-rabbit IgG antibodies with conjugated alkaline phosphatase (Sigma-Aldrich, Germany).

Absorbance-Based Assay for the Determination of Decarboxylase Activity. The assay was performed as previously described.[68] In brief, 50 μL of a 0.1 μM enzyme solution in PAD buffer was transferred in an ultraviolet (UV) transparent 96-well microtiter plate, and 150 μL of a *p*-coumaric acid (*p*CA) stock to a final concentration of 0.1 mM in PAD buffer was added. The consumption of *p*CA was recorded at 294 nm by using a Synergy MX microplate reader (BioTek, Winooski, VT) over a period of 20 min at 30 °C. Activity was calculated from the linear decrease in absorption intensity and the calibration curve shown in Figure S7. All measurements were performed at least six times in biological

https://doi.org/10.1021/acsami.2c03337
ACS Appl. Mater. Interfaces 2022, 14, 22138−22150

duplicates. For calibration curves and as positive control, *p*-hydroxystyrene (*p*HS) was synthesized as described previously.[46,93]

Determination of Decarboxylase Activity via High Performance Liquid Chromatography (HPLC). Specific enzyme activity was analyzed via HPLC. In a 1.5 mL reaction tube, 25 μL of a 4 μM solution of the corresponding PAD variant in PAD buffer (25 mM potassium phosphate, pH 6) or 25 μL containing PAD immobilized on beads were added to 725 μL of PAD buffer. After preincubation at 30 °C and 600 rpm, the reaction was started by addition of 250 μL of a 5 mM *p*CA stock solution in PAD buffer by using DMSO as cosolvent. The final substrate concentration was 1.25 mM. Time-dependent samples of 100 μL reaction solution were taken manually, quenched with 100 μL of quenching solution (1 mM cinnamic acid as internal standard, 25 mM HCl in aqueous acetonitrile) and incubated at 50 °C under vigorous shaking for 10 min to quench the enzymatic activity. The samples were centrifuged, and the supernatant was transferred to HPLC vials for further analysis. HPLC analyses were performed on an Agilent Technologies (Palo Alto, CA) 1100 Series with autosampler and diode array detector (DAD). *p*HS and *p*CA were detected and quantified by reverse phase HPLC using an Eclipse XDB C18 column (5 μm, Agilent) with a precolumn of the same material, with cinnamic acid as internal standard (Figure S8). The separation was realized at 10 °C with a gradient method: solvent A: acetonitrile; solvent B: ddH_2O with 0.1% (v/v) trifluoroacetic acid; gradient: 0 min 35% A 65% B; injection volume: 10 μL; flow rate: 1 mL min^{-1}). Chromatograms were recorded at 254 nm (*p*HS) and 284 nm (*p*CA and cinnamic acid). For calibration, dilutions of *p*HS and *p*CA in the range of 0.1−5 mM were prepared in PAD buffer, diluted with quenching solution as described above, and subjected to HPLC analysis (Figures S9 and S10).

■ ASSOCIATED CONTENT

Supporting Information

The Supporting Information is available free of charge at https://pubs.acs.org/doi/10.1021/acsami.2c03337.

Additional data and discussion: schematics illustrating the construction of the *mamC-spycatcher* gene fusion; immunochemical detection of MamC-SC and calculations regarding the copy number of EGFP-ST immobilized on SC-magnetosomes; illustration of the preparation of the immobilized biocatalysts used in this study; integrity and size distribution of SC-magnetosomes before and after application in a flow reactor; comparative enzyme stability of free PAD-ST in batch and on SC-magnetosomes in a flow reactor; calibration curves and chromatograms for HPLC analysis used in this study; additional experimental details and methods; information about strains and plasmids and protein and oligonucleotide sequences used in this study (PDF)

■ AUTHOR INFORMATION

Corresponding Authors

Kersten S. Rabe − *Institute for Biological Interfaces 1, Karlsruhe Institute of Technology (KIT), D-76344 Eggenstein-Leopoldshafen, Germany;* orcid.org/0000-0001-7909-8191; Email: kersten.rabe@kit.edu

Dirk Schüler − *Department of Microbiology, University of Bayreuth, D-95447 Bayreuth, Germany;* Email: dirk.schueler@uni-bayreuth.de

Authors

Esther Mittmann − *Institute for Biological Interfaces 1, Karlsruhe Institute of Technology (KIT), D-76344 Eggenstein-Leopoldshafen, Germany;* orcid.org/0000-0001-5642-1232

Frank Mickoleit − *Department of Microbiology, University of Bayreuth, D-95447 Bayreuth, Germany;* orcid.org/0000-0002-1943-3960

Denis S. Maier − *Department of Microbiology, University of Bayreuth, D-95447 Bayreuth, Germany*

Sabrina Y. Stäbler − *Department of Microbiology, University of Bayreuth, D-95447 Bayreuth, Germany;* orcid.org/0000-0001-8243-3587

Marius A. Klein − *Department of Microbiology, University of Bayreuth, D-95447 Bayreuth, Germany*

Christof M. Niemeyer − *Institute for Biological Interfaces 1, Karlsruhe Institute of Technology (KIT), D-76344 Eggenstein-Leopoldshafen, Germany;* orcid.org/0000-0002-8837-081X

Complete contact information is available at: https://pubs.acs.org/10.1021/acsami.2c03337

Author Contributions

E.M. and F.M. contributed equally to this work.

Notes

The authors declare no competing financial interest.

■ ACKNOWLEDGMENTS

The authors are grateful to Sarah Borg for providing expression plasmids and Matthias Schlotter (Department of Microbiology, University of Bayreuth) for technical assistance with cell cultivation, magnetosome isolation, and iron measurements. Laura Schönbrodt is acknowledged for contributing some of the data produced as part of her Bachelor's thesis at the Department of Microbiology (University of Bayreuth). We also thank Maike Bohnhorst, Svenja Moench, Julian Hertel, Sabrina Gallus, and Martin Peng (IBG-1, Karlsruhe Institute of Technology) for their experimental help. Funding was received in part from the European Research Council (ERC) under the European Union's Horizon 2020 research and innovation program (Grant No. 692637 to D.S.) and from the Federal Ministry of Education and Research (BMBF, grant MagBioFab to D.S.). This work was also supported through the Helmholtz program "Materials Systems Engineering" under the topic "Adaptive and Bioinstructive Materials Systems".

■ REFERENCES

(1) Wu, S. K.; Snajdrova, R.; Moore, J. C.; Baldenius, K.; Bornscheuer, U. T. Biocatalysis: Enzymatic Synthesis for Industrial Applications. *Angew. Chem., Int. Ed. Engl.* **2021**, *60* (1), 88−119.

(2) Hauer, B. Embracing Nature's Catalysts: A Viewpoint on the Future of Biocatalysis. *ACS Catal.* **2020**, *10* (15), 8418−8427.

(3) Sheldon, R. A. A.; Brady, D.; Bode, M. L. L. The Hitchhiker's guide to biocatalysis: recent advances in the use of enzymes in organic synthesis. *Chem. Sci.* **2020**, *11* (10), 2587−2605.

(4) Sheldon, R. A.; Woodley, J. M. Role of Biocatalysis in Sustainable Chemistry. *Chem. Rev.* **2018**, *118* (2), 801−838.

(5) Rabe, K. S.; Muller, J.; Skoupi, M.; Niemeyer, C. M. Cascades in Compartments: En Route to Machine-Assisted Biotechnology. *Angew. Chem., Int. Ed. Engl.* **2017**, *56* (44), 13574−13589.

(6) Cardoso Marques, M. P.; Lorente-Arevalo, A.; Bolivar, J. M. Biocatalysis in Continuous-Flow Microfluidic Reactors. *Adv. Biochem. Eng. Biotechnol.* **2021**, DOI: 10.1007/10_2020_160.

(7) Peschke, T.; Bitterwolf, P.; Gallus, S.; Hu, Y.; Oelschlaeger, C.; Willenbacher, N.; Rabe, K. S.; Niemeyer, C. M. Self-Assembling All-Enzyme Hydrogels for Flow Biocatalysis. *Angew. Chem., Int. Ed. Engl.* **2018**, *57* (52), 17028−17032.

(8) Zhu, Y. J.; Chen, Q. M.; Shao, L. Y.; Jia, Y. W.; Zhang, X. M. Microfluidic immobilized enzyme reactors for continuous biocatalysis. *React. Chem. Eng.* **2020**, *5* (1), 9−32.
(9) Peschke, T.; Bitterwolf, P.; Rabe, K. S.; Niemeyer, C. M. Self-Immobilizing Oxidoreductases for Flow Biocatalysis in Miniaturized Packed-Bed Reactors. *Chem. Eng. Technol.* **2019**, *42* (10), 2009−2017.
(10) Lindeque, R. M.; Woodley, J. M. Reactor Selection for Effective Continuous Biocatalytic Production of Pharmaceuticals. *Catalysts* **2019**, *9* (3), 262.
(11) Zhang, M.; Ettelaie, R.; Dong, L.; Li, X.; Li, T.; Zhang, X.; Binks, B. P.; Yang, H. Pickering emulsion droplet-based biomimetic microreactors for continuous flow cascade reactions. *Nat. Commun.* **2022**, *13* (1), 475.
(12) Heyse, A.; Plikat, C.; Ansorge-Schumacher, M.; Drews, A. Continuous two-phase biocatalysis using water-in-oil Pickering emulsions in a membrane reactor: Evaluation of different nanoparticles. *Catal. Today* **2019**, *331*, 60−67.
(13) Sheldon, R. A.; Basso, A.; Brady, D. New frontiers in enzyme immobilisation: robust biocatalysts for a circular bio-based economy. *Chem. Soc. Rev.* **2021**, *50* (10), 5850−5862.
(14) Peschke, T.; Skoupi, M.; Burgahn, T.; Gallus, S.; Ahmed, I.; Rabe, K. S.; Niemeyer, C. M. Self-Immobilizing Fusion Enzymes for Compartmentalized Biocatalysis. *ACS Catal.* **2017**, *7* (11), 7866−7872.
(15) Sastre, D. E.; Reis, E. A.; Marques Netto, C. G. C. Strategies to rationalize enzyme immobilization procedures. *Methods Enzymol* **2020**, *630*, 81−110.
(16) Peschke, T.; Rabe, K. S.; Niemeyer, C. M. Orthogonal Surface Tags for Whole-Cell Biocatalysis. *Angew. Chem., Int. Ed. Engl.* **2017**, *56* (8), 2183−2186.
(17) Bollella, P.; Katz, E. Chapter One - Magneto-controlled enzyme reactions. In *Methods in Enzymology*; Kumar, C. V., Ed.; Academic Press: 2020; Vol. *630*, pp 1−24.
(18) Peschke, T.; Bitterwolf, P.; Hansen, S.; Gasmi, J.; Rabe, K. S.; Niemeyer, C. M. Self-Immobilizing Biocatalysts Maximize Space−Time Yields in Flow Reactors. *Catalysts* **2019**, *9* (2), 164.
(19) Žnidaršič-Plazl, P. Biocatalytic process intensification via efficient biocatalyst immobilization, miniaturization, and process integration. *Curr. Opin. Green Sustain. Chem.* **2021**, *32*, 100546.
(20) Valikhani, D.; Bolivar, J. M.; Viefhues, M.; McIlroy, D. N.; Vrouwe, E. X.; Nidetzky, B. A Spring in Performance: Silica Nanosprings Boost Enzyme Immobilization in Microfluidic Channels. *ACS Appl. Mater. Interfaces* **2017**, *9* (40), 34641−34649.
(21) Uebe, R.; Schuler, D. Magnetosome biogenesis in magnetotactic bacteria. *Nat. Rev. Microbiol.* **2016**, *14* (10), 621−37.
(22) Schüler, D.; Müller, F. D. Biosynthesis and Intracellular Organization of Magnetosomes in Magnetotactic Bacteria. In *Bacterial Organelles and Organelle-like Inclusions*; Jendrossek, D., Ed.; Springer International Publishing: Cham, 2020; pp 53−70.
(23) Faivre, D.; Schüler, D. Magnetotactic Bacteria and Magnetosomes. *Chem. Rev.* **2008**, *108* (11), 4875−4898.
(24) Staniland, S. S.; Rawlings, A. E. Crystallizing the function of the magnetosome membrane mineralization protein Mms6. *Biochem. Soc. Trans.* **2016**, *44* (3), 883−890.
(25) Staniland, S.; Ward, B.; Harrison, A.; van der Laan, G.; Telling, N. Rapid magnetosome formation shown by real-time x-ray magnetic circular dichroism. *Proc. Natl. Acad. Sci. U. S. A.* **2007**, *104* (49), 19524−19528.
(26) Alphandéry, E. Applications of Magnetosomes Synthesized by Magnetotactic Bacteria in Medicine. *Front. Bioeng. Biotechnol.* **2014**.
(27) Vargas, G.; Cypriano, J.; Correa, T.; Leão, P.; Bazylinski, D. A.; Abreu, F. Applications of Magnetotactic Bacteria, Magnetosomes and Magnetosome Crystals in Biotechnology and Nanotechnology: Mini-Review. *Molecules* **2018**, *23* (10), 2438.
(28) Sun, J.-B.; Duan, J.-H.; Dai, S.-L.; Ren, J.; Guo, L.; Jiang, W.; Li, Y. Preparation and anti-tumor efficiency evaluation of doxorubicin-loaded bacterial magnetosomes: Magnetic nanoparticles as drug carriers isolated from Magnetospirillum gryphiswaldense. *Biotechnol. Bioeng.* **2008**, *101* (6), 1313−1320.
(29) Mickoleit, F.; Lanzloth, C.; Schüler, D. A Versatile Toolkit for Controllable and Highly Selective Multifunctionalization of Bacterial Magnetic Nanoparticles. *Small* **2020**, *16* (16), 1906922.
(30) Gao, J.; Gu, H.; Xu, B. Multifunctional Magnetic Nanoparticles: Design, Synthesis, and Biomedical Applications. *Acc. Chem. Res.* **2009**, *42* (8), 1097−1107.
(31) Borg, S.; Hofmann, J.; Pollithy, A.; Lang, C.; Schüler, D. New vectors for chromosomal integration enable high-level constitutive or inducible magnetosome expression of fusion proteins in Magnetospirillum gryphiswaldense. *Appl. Environ. Microbiol.* **2014**, *80* (8), 2609−16.
(32) Takahashi, M.; Yoshino, T.; Matsunaga, T. Surface modification of magnetic nanoparticles using asparagines-serine polypeptide designed to control interactions with cell surfaces. *Biomaterials* **2010**, *31* (18), 4952−7.
(33) Mickoleit, F.; Borkner, C. B.; Toro-Nahuelpan, M.; Herold, H. M.; Maier, D. S.; Plitzko, J. M.; Scheibel, T.; Schüler, D. In Vivo Coating of Bacterial Magnetic Nanoparticles by Magnetosome Expression of Spider Silk-Inspired Peptides. *Biomacromolecules* **2018**, *19* (3), 962−972.
(34) Xu, J.; Liu, L.; He, J.; Ma, S.; Li, S.; Wang, Z.; Xu, T.; Jiang, W.; Wen, Y.; Li, Y.; Tian, J.; Li, F. Engineered magnetosomes fused to functional molecule (protein A) provide a highly effective alternative to commercial immunomagnetic beads. *J. Nanobiotechnol.* **2019**, *17* (1), 37.
(35) Lang, C.; Schüler, D. Expression of Green Fluorescent Protein Fused to Magnetosome Proteins in Microaerophilic Magnetotactic Bacteria. *Appl. Environ. Microbiol.* **2008**, *74* (15), 4944−4953.
(36) Ginet, N.; Pardoux, R.; Adryanczyk, G.; Garcia, D.; Brutesco, C.; Pignol, D. Single-Step Production of a Recyclable Nanobiocatalyst for Organophosphate Pesticides Biodegradation Using Functionalized Bacterial Magnetosomes. *PLoS One* **2011**, *6* (6), e21442.
(37) Mickoleit, F.; Schüler, D. Generation of Multifunctional Magnetic Nanoparticles with Amplified Catalytic Activities by Genetic Expression of Enzyme Arrays on Bacterial Magnetosomes. *Adv. Biosyst* **2018**, *2* (1), 1700109.
(38) Borg, S.; Popp, F.; Hofmann, J.; Leonhardt, H.; Rothbauer, U.; Schuler, D. An Intracellular Nanotrap Redirects Proteins and Organelles in Live Bacteria. *mBio* **2015**, *6* (1), e02117−14.
(39) Mickoleit, F.; Altintoprak, K.; Wenz, N. L.; Richter, R.; Wege, C.; Schüler, D. Precise Assembly of Genetically Functionalized Magnetosomes and Tobacco Mosaic Virus Particles Generates a Magnetic Biocomposite. *ACS Appl. Mater. Interfaces* **2018**, *10* (44), 37898−37910.
(40) Mickoleit, F.; Jérôme, V.; Freitag, R.; Schüler, D. Bacterial Magnetosomes as Novel Platform for the Presentation of Immunostimulatory, Membrane-Bound Ligands in Cellular Biotechnology. *Adv. Biosyst.* **2020**, *4* (3), e1900231.
(41) Ceyhan, B.; Alhorn, P.; Lang, C.; Schüler, D.; Niemeyer, C. M. Semisynthetic biogenic magnetosome nanoparticles for the detection of proteins and nucleic acids. *Small* **2006**, *2* (11), 1251−5.
(42) Amelung, S.; Nerlich, A.; Rohde, M.; Spellerberg, B.; Cole, J. N.; Nizet, V.; Chhatwal, G. S.; Talay, S. R. The FbaB-type fibronectin-binding protein of Streptococcus pyogenes promotes specific invasion into endothelial cells. *Cell. Microbiol.* **2011**, *13* (8), 1200−11.
(43) Zakeri, B.; Fierer, J. O.; Celik, E.; Chittock, E. C.; Schwarz-Linek, U.; Moy, V. T.; Howarth, M. Peptide tag forming a rapid covalent bond to a protein, through engineering a bacterial adhesin. *Proc. Natl. Acad. Sci. U. S. A.* **2012**, *109* (12), E690−E697.
(44) Reddington, S. C.; Howarth, M. Secrets of a covalent interaction for biomaterials and biotechnology: SpyTag and SpyCatcher. *Curr. Opin. Chem. Biol.* **2015**, *29*, 94−9.
(45) Zakeri, B. Synthetic Biology: A New Tool for the Trade. *ChemBioChem* **2015**, *16* (16), 2277−82.
(46) Mittmann, E.; Gallus, S.; Bitterwolf, P.; Oelschlaeger, C.; Willenbacher, N.; Niemeyer, C. M.; Rabe, K. S. A Phenolic Acid Decarboxylase-Based All-Enzyme Hydrogel for Flow Reactor Technology. *Micromachines* **2019**, *10* (12), 795.

(47) Gallus, S.; Mittmann, E.; Rabe, K. S. A Modular System for the Rapid Comparison of Different Membrane Anchors for Surface Display on Escherichia coli. *ChemBioChem* **2022**, DOI: 10.1002/cbic.202100472.
(48) Bao, J.; Liu, N.; Zhu, L.; Xu, Q.; Huang, H.; Jiang, L. Programming a Biofilm-Mediated Multienzyme-Assembly-Cascade System for the Biocatalytic Production of Glucosamine from Chitin. *J. Agric. Food Chem.* **2018**, *66* (30), 8061−8068.
(49) Alam, M. K.; Gonzalez, C.; Hill, W.; El-Sayed, A.; Fonge, H.; Barreto, K.; Geyer, C. R. Synthetic Modular Antibody Construction by Using the SpyTag/SpyCatcher Protein-Ligase System. *ChemBioChem* **2017**, *18* (22), 2217−2221.
(50) Brune, K. D.; Leneghan, D. B.; Brian, I. J.; Ishizuka, A. S.; Bachmann, M. F.; Draper, S. J.; Biswas, S.; Howarth, M. Plug-and-Display: decoration of Virus-Like Particles via isopeptide bonds for modular immunization. *Sci. Rep.* **2016**, *6*, 19234.
(51) Jia, L.; Minamihata, K.; Ichinose, H.; Tsumoto, K.; Kamiya, N. Polymeric SpyCatcher Scaffold Enables Bioconjugation in a Ratio-Controllable Manner. *Biotechnol. J.* **2017**, *12* (12), 1700195.
(52) Ma, W.; Saccardo, A.; Roccatano, D.; Aboagye-Mensah, D.; Alkaseem, M.; Jewkes, M.; Di Nezza, F.; Baron, M.; Soloviev, M.; Ferrari, E. Modular assembly of proteins on nanoparticles. *Nat. Commun.* **2018**, *9* (1), 1489.
(53) Peng, M.; Siebert, D. L.; Engqvist, M. K. M.; Niemeyer, C. M.; Rabe, K. S. Modeling-Assisted Design of Thermostable Benzaldehyde Lyases from Rhodococcus erythropolis for Continuous Production of α-Hydroxy Ketones. *ChemBioChem* **2022**.
(54) Thrane, S.; Janitzek, C. M.; Matondo, S.; Resende, M.; Gustavsson, T.; de Jongh, W. A.; Clemmensen, S.; Roeffen, W.; van de Vegte-Bolmer, M.; van Gemert, G. J.; Sauerwein, R.; Schiller, J. T.; Nielsen, M. A.; Theander, T. G.; Salanti, A.; Sander, A. F. Bacterial superglue enables easy development of efficient virus-like particle based vaccines. *J. Nanobiotechnol.* **2016**, *14*, 30.
(55) van den Berg van Saparoea, H. B.; Houben, D.; de Jonge, M. I.; Jong, W. S. P.; Luirink, J. Display of Recombinant Proteins on Bacterial Outer Membrane Vesicles by Using Protein Ligation. *Appl. Environ. Microbiol.* **2018**, DOI: 10.1128/AEM.02567-17.
(56) Zhang, G.; Quin, M. B.; Schmidt-Dannert, C. Self-Assembling Protein Scaffold System for Easy in Vitro Coimmobilization of Biocatalytic Cascade Enzymes. *ACS Catal.* **2018**, *8* (6), 5611−5620.
(57) Moon, H.; Bae, Y.; Kim, H.; Kang, S. Plug-and-playable fluorescent cell imaging modular toolkits using the bacterial superglue, SpyTag/SpyCatcher. *Chem. Commun.* **2016**, *52* (97), 14051−14054.
(58) Pessino, V.; Citron, Y. R.; Feng, S.; Huang, B. Covalent Protein Labeling by SpyTag-SpyCatcher in Fixed Cells for Super-Resolution Microscopy. *ChemBioChem* **2017**, *18* (15), 1492−1495.
(59) Pröschel, M.; Detsch, R.; Boccaccini, A. R.; Sonnewald, U. Engineering of Metabolic Pathways by Artificial Enzyme Channels. *Front. Bioeng. Biotechnol.* **2015**, *3*, 168.
(60) Grünberg, K.; Wawer, C.; Tebo, B. M.; Schüler, D. A large gene cluster encoding several magnetosome proteins is conserved in different species of magnetotactic bacteria. *Appl. Environ. Microbiol.* **2001**, *67* (10), 4573−82.
(61) Grünberg, K.; Müller, E.-C.; Otto, A.; Reszka, R.; Linder, D.; Kube, M.; Reinhardt, R.; Schüler, D. Biochemical and Proteomic Analysis of the Magnetosome Membrane in *Magnetospirillum gryphiswaldense*. *Appl. Environ. Microbiol.* **2004**, *70* (2), 1040−1050.
(62) Nudelman, H.; Zarivach, R. Structure prediction of magneto-some-associated proteins. *Front. Microbiol.* **2014**.
(63) Raschdorf, O.; Bonn, F.; Zeytuni, N.; Zarivach, R.; Becher, D.; Schüler, D. A quantitative assessment of the membrane-integral sub-proteome of a bacterial magnetic organelle. *J. Proteomics* **2018**, *172*, 89−99.
(64) Scheffel, A.; Gärdes, A.; Grünberg, K.; Wanner, G.; Schüler, D. The Major Magnetosome Proteins MamGFDC Are Not Essential for Magnetite Biomineralization in *Magnetospirillum gryphiswaldense* but Regulate the Size of Magnetosome Crystals. *J. Bacteriol. Res.* **2008**, *190* (1), 377−386.
(65) Mickoleit, F.; Schüler, D. Generation of nanomagnetic biocomposites by genetic engineering of bacterial magnetosomes. *Bioinspired Biomim. Nanobiomater.* **2019**, *8* (1), 86−98.
(66) Burgahn, T.; Pietrek, P.; Dittmeyer, R.; Rabe, K. S.; Niemeyer, C. M. Evaluation of a Microreactor for Flow Biocatalysis by Combined Theory and Experiment. *ChemCatChem* **2020**, *12* (9), 2452−2460.
(67) Gu, W.; Yang, J.; Lou, Z.; Liang, L.; Sun, Y.; Huang, J.; Li, X.; Cao, Y.; Meng, Z.; Zhang, K. Q. Structural basis of enzymatic activity for the ferulic acid decarboxylase (FADase) from Enterobacter sp. Px6−4. *PLoS One* **2011**, *6* (1), e16262.
(68) Peng, M.; Mittmann, E.; Wenger, L.; Hubbuch, J.; Engqvist, M. K. M.; Niemeyer, C. M.; Rabe, K. S. 3D-Printed Phenacrylate Decarboxylase Flow Reactors for the Chemoenzymatic Synthesis of 4-Hydroxystilbene. *Chem.—Eur. J.* **2019**, *25* (70), 15998−16001.
(69) Burgahn, T.; Garrecht, R.; Rabe, K. S.; Niemeyer, C. M. Solid-Phase Synthesis and Purification of Protein−DNA Origami Nanostructures. *Chem.—Eur. J.* **2019**, *25* (14), 3483−3488.
(70) Lauback, S.; Mattioli, K. R.; Marras, A. E.; Armstrong, M.; Rudibaugh, T. P.; Sooryakumar, R.; Castro, C. E. Real-time magnetic actuation of DNA nanodevices via modular integration with stiff micro-levers. *Nat. Commun.* **2018**, *9* (1), 1446.
(71) Yung, C. W.; Fiering, J.; Mueller, A. J.; Ingber, D. E. Micromagnetic−microfluidic blood cleansing device. *Lab Chip* **2009**, *9* (9), 1171−1177.
(72) Koßmann, K. J.; Ziegler, C.; Angelin, A.; Meyer, R.; Skoupi, M.; Rabe, K. S.; Niemeyer, C. M. A Rationally Designed Connector for Assembly of Protein-Functionalized DNA Nanostructures. *ChemBioChem* **2016**, *17* (12), 1102−1106.
(73) Kröll, S.; Rabe, K. S.; Niemeyer, C. M. An Orthogonal Covalent Connector System for the Efficient Assembly of Enzyme Cascades on DNA Nanostructures. *Small* **2021**, *17* (51), 2105095.
(74) Inc., T. F. S. Dynabeads M-270 Epoxy. https://www.thermofisher.com/order/catalog/product/14302D?SID=srch-srp-14302D (accessed Nov 2021).
(75) Inc., T. F. S. Dynabeads M-280 Streptavidin. https://www.thermofisher.com/order/catalog/product/11205D (accessed Nov 2021).
(76) Charalambous, A.; Antoniades, I.; Christodoulou, N.; Skourides, P. A. Split-Inteins for Simultaneous, site-specific conjugation of Quantum Dots to multiple protein targets In vivo. *J. Nanobiotechnol.* **2011**, *9* (1), 37.
(77) De Crescenzo, G.; Litowski, J. R.; Hodges, R. S.; O'Connor-McCourt, M. D. Real-time monitoring of the interactions of two-stranded de novo designed coiled-coils: effect of chain length on the kinetic and thermodynamic constants of binding. *Biochem* **2003**, *42* (6), 1754−63.
(78) Blakeley, B. D.; Chapman, A. M.; McNaughton, B. R. Split-superpositive GFP reassembly is a fast, efficient, and robust method for detecting protein-protein interactions in vivo. *Mol. Biosyst* **2012**, *8* (8), 2036−40.
(79) Pollithy, A.; Romer, T.; Lang, C.; Müller, F. D.; Helma, J.; Leonhardt, H.; Rothbauer, U.; Schüler, D. Magnetosome Expression of Functional Camelid Antibody Fragments (Nanobodies) in Magnetospirillum gryphiswaldense. *Appl. Environ. Microbiol.* **2011**, *77* (17), 6165−6171.
(80) Heyen, U.; Schüler, D. Growth and magnetosome formation by microaerophilic Magnetospirillum strains in an oxygen-controlled fermentor. *Appl. Microbiol. Biotechnol.* **2003**, *61* (5−6), 536−44.
(81) Lang, C.; Schüler, D. Expression of green fluorescent protein fused to magnetosome proteins in microaerophilic magnetotactic bacteria. *Appl. Environ. Microbiol.* **2008**, *74* (15), 4944−53.
(82) Gibson, D. G.; Young, L.; Chuang, R. Y.; Venter, J. C.; Hutchison, C. A.; Smith, H. O. Enzymatic assembly of DNA molecules up to several hundred kilobases. *Nat. Methods* **2009**, *6* (5), 343−U41.
(83) Maruyama, F.; Watanabe, T.; Nakagawa, I. Streptococcus pyogenes Genomics. In *Streptococcus Pyogenes: Basic Biology to Clinical Manifestations*; Ferretti, J. J., Stevens, D. L., Fischetti, V. A., Eds.; The

University of Oklahoma Health Sciences Center: Oklahoma City, OK, 2016.
(84) Robinson, C. R.; Sauer, R. T. Optimizing the stability of single-chain proteins by linker length and composition mutagenesis. *Proc. Natl. Acad. Sci. U. S. A.* **1998**, *95* (11), 5929−5934.
(85) Bryksin, A. V.; Matsumura, I. Overlap extension PCR cloning: a simple and reliable way to create recombinant plasmids. *BioTechniques* **2010**, *48* (6), 463−5.
(86) Rosenfeldt, S.; Mickoleit, F.; Jörke, C.; Clement, J. H.; Markert, S.; Jérôme, V.; Schwarzinger, S.; Freitag, R.; Schüler, D.; Uebe, R.; Schenk, A. S. Towards standardized purification of bacterial magnetic nanoparticles for future in vivo applications. *Acta Biomater.* **2021**, *120*, 293−303.
(87) Spriestersbach, A.; Kubicek, J.; Schäfer, F.; Block, H.; Maertens, B. Purification of His-Tagged Proteins. *Methods Enzymol.* **2015**, *559*, 1−15.
(88) Schmitt, J.; Hess, H.; Stunnenberg, H. G. Affinity purification of histidine-tagged proteins. *Mol. Biol. Rep.* **1993**, *18* (3), 223−30.
(89) Schüler, D.; Uhl, R.; Bäuerlein, E. A simple light scattering method to assay magnetism in Magnetospirillum gryphiswaldense. *FEMS Microbiol. Lett.* **1995**, *132* (1−2), 139−145.
(90) Collins, T. J. ImageJ for microscopy. *BioTechniques* **2007**, *43* (1), 25−30.
(91) Laemmli, U. K. Cleavage of structural proteins during the assembly of the head of bacteriophage T4. *Nature* **1970**, *227* (5259), 680−5.
(92) Fling, S. P.; Gregerson, D. S. Peptide and protein molecular weight determination by electrophoresis using a high-molarity tris buffer system without urea. *Anal. Biochem.* **1986**, *155* (1), 83−8.
(93) Demidoff, F. C.; de Souza, F. P.; Netto, C. D. Synthesis of Stilbene-Quinone Hybrids through Heck Reactions in PEG-400. *Synthesis* **2017**, *49* (23), 5217−5223.

https://doi.org/10.1021/acsami.2c03337
ACS Appl. Mater. Interfaces 2022, 14, 22138−22150